PORT-SAID ENGINEERING RESEARCH JOURNAL
Faculty of Engineering - Port Said University
Volume 23 No. 1 March 2019 pp: 94:105

A Numerical Study of the Effect of Endwall Injection Inclination Angle on a High Pressure Turbine Cascade Performance

Alam El-Din, A. M.[1], *El-Ghandour, M. E.*[2], *Hassan, Y. K.*[3]

ABSTRACT

The turbine flow near the endwall is highly three-dimensional flow. The injection flow has been investigated widely as an effective way to increase turbine efficiency. For the current study, the interaction between the main flow and the injection control flow from flat endwall, is analyzed by numerical simulation. Flow injection were done using five endwall holes placed on a typical flat blade cascade near the blade suction side with six different inclination angles arrangements. In these test cases all the five holes has the same inclination angle. In addition, two new injection test cases, namely, mixing inclination angles in which each hole has an inclination angle independent of other holes. The new injection arrangements techniques have proved its effectiveness in increasing blade loading by 1.71 % more than baseline test case blade loading. Also, it proved its effectiveness in suppressing the flow losses by 2.1 % less than baseline test case losses. Moreover, all selected test cases gave positive different readings with respect to blade loading by increasing the static pressure on the blade surface and preventing boundary layer separation at the suction side and hence reducing the large undesirable effects of secondary flows.

1. INTRODUCTION

An important problem that arises in the design and the performance of axial flow turbines is the understanding, analysis, prediction and control of secondary flows. Customarily, primary or uniform flow is an idealized two-dimensional form of the streamlines between the suction and pressure surfaces of a turbine blade passage. Flow deviations from the idealized form have come to be called "secondary", even though their presence may constitute whole regions of the turbine blade passage flow field. Secondary flows include endwall boundary layers, their separation, and other portions of the primary flow influenced by three-dimensional effects. During the last two decades, mastery of secondary flow phenomenon has become critical to modern turbine designs [1].

Gregory-Smith and Okan [2] describe the basic physics behind the generation of the passage vortex. When a sheared flow such as a boundary layer forced around a turn the slower moving fluid follows a tighter radius of curvature, leading to a tangential flow across the passage. Then, in order to preserve continuity, a vertical flow is formed. Langston [3] presented a classic secondary flow model based on detail experimental measurements in a turbine cascade [4], and also presented that the secondary flow in turbine passage consisted of three kinds of flow components such as the passage vortex, the corner vortex and the horse shoe vortex is splitting into a pressure side leg and a suction side leg (and tip leakage vortex in rotor blade passage).

[1] Professor, Mech. Power Dept., Faculty of Engineering, Port Said University, Port Said, Egypt, Email: atef_alameldin@yahoo.com
[2] Lecturer, Mech. Power Dept., Faculty of Engineering, Port Said University, Port Said, Egypt, Email: mghandour@eng.psu.edu.eg
[3] Researcher, Mech. Power Dept., Faculty of Engineering, Port Said University, Port Said, Egypt, Email: yasserkamal@eng.psu.edu.eg

edge of the airfoil by rolling up of the boundary layer, and transform to horseshoe vortex when it spreads to the whole passage. The migration and development of the vortex through the entire passage indicate their importance in the overall aerodynamic losses.

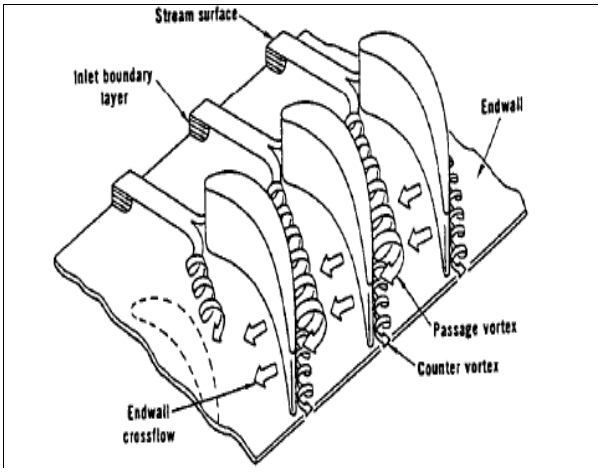

Fig. 1: Secondary Flow Model of Langston [3]

When the boundary layer fluid approaches the blade leading edge, it is subjected to an adverse pressure gradient and starts to roll up to form a horse shoe vortex with two legs [3], as shown in Fig. 1, one to pressure side (move away from the pressure surface and toward the suction surface of the adjacent blade to be the major component of the passage vortex) and the other to suction side (travels along the suction surface toward the trailing edge), it moves away from the endwall toward the midspan and downstream to the separation bubble and hence increase the losses [5].

Secondary flow controlling methods according to most of previous studies are mainly classified to two

categories, the first category is dealing with structural measures in blade or endwall geometry and the second category is dealing with injection or suction of air directly to the flow passage.

Turbine blade loading, (L), is the main output of gas turbine Engine which is the main reason for turbine disk rotation then introducing a flow or mechanical power to service a specific part of the engine. The blade loading or lift (equation 1) that provides work on the turbine shaft is determined for blade cross section at certain span distance based on the area of integration of local static pressure at every point on blade surface cross section chordwisely from Leading edge to trailing edge [6].

$$\mathcal{L} = \frac{1}{2}\rho A v^2 C_L \quad (1)$$

The blowing ratio $M_{h-inlet}$ (equation 2) is the ratio that an idealized loss free injection hole would have when injecting to inlet conditions [7].

$$M_{h-inlet} = \frac{(\dot{m}_{inj}/A_{holes})}{\rho_\infty . U_\infty} \quad (2)$$

The compound angle of injection hole has two injection angles as shown in Fig. 2 [8]. In the compound angle orientation system, the injected flow is injected with spanwise, chorwise and pitchwise momentum components.

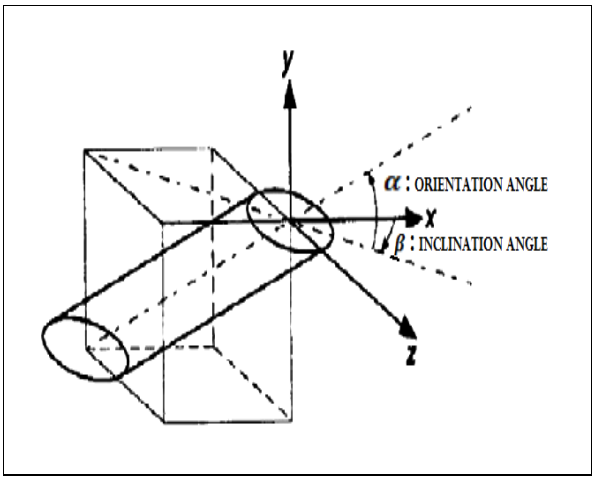

Fig. 2: Injection hole compound angle [8]

The inclination angle (β_h) is defined as the angle between the injection vector and its projection on the x–z plane, whereas the orientation angle (α_h) is defined as the angle between the streamwise direction and the projection of the injection vector on the x–y plane.

Pu and Hua [9] applied a row of converging slot-holes upstream of a linear GE-E3 high pressure turbine cascade to enhance film-cooling effect in end-wall leading edge region and weaken secondary vortices. The effects of geometric parameters of the converging hole-slot, including inclination angle and outlet-to-inlet area ratio, on time-mean characteristics of secondary vortices and adiabatic film-cooling effectiveness, are investigated. Three types of converging slot-holes with two different area ratios (area ratio = outlet area to inlet area of slot hole) they used inclination angles of β_h = 30° and 65°. The comparison reveals that, the secondary vortices can be weakened by the coolant injection from the cylindrical hole only at higher blowing ratios; however, the 30° converging slot-holes has a potential to simultaneously improve end-wall cooling effect and weaken the secondary vortices.

Qing et al. [10] investigated the contoured endwall as an effective way to increase the turbine efficiency by mitigating the strength of vortices. But the injection flow effectiveness may be greatly changed as the surface curvature is an important factor affecting the film cooling performance. A round hole and a diffused hole are arranged on both flat endwall and contoured endwall with different hole shapes and with various inclination angles. Results showed a higher but a faster decline on film effectiveness of diffused hole than the round hole in the same condition.

2. MODEL STUDY

This numerical study is carried out to establish the effect of mixing inclination angles of endwall injection on a high pressure turbine cascade performance through flow channel between two consecutives blades by simulating a large scale transonic turbine blade cascade. Detailed measurements, made by Ashlie et al. [11], are used for validation of the CFD results by using the same inlet flow conditions and existing blade geometry. The test blade is a scaled rotor tip section of the GE Energy Efficient Engine (EEE) design [12], that has an axial chord of 130.0 mm, a blade pitch of 130.0 mm, a span of 152.4 mm, and a design-intent inlet flow angle of $\beta_{1,des}$ = +29.7° with inlet conditions as shown in Table 1. This blade geometry was considered to be a good test case because direct comparisons could be made between data obtained by Ashlie et al experimental results and the current study CFD results.

Table 1: Experimental inlet conditions, Ashlie et al. [11]

Inlet conditions	
β_1 Relative flow angle	38.8 °
i Incidence angle, $i = \beta_1 - \beta_{1,des}$	+9.1 °
$Re_{Cx,1}$	685,300
PR Pressure Ratio, PR = $P_{t1}/\overline{P_2}$	1.4472
$M_{2,i}$ Mach number	0.746
Est. δ_1 Boundary layer thickness, m	0.0326

The injection location is selected at blade aft suction side (the region of separation), the selection of these particular locations is based to higher blade loading results and relatively low losses results in experiment test study Alam El-Din et al. [13].

3. MATHEMATICAL MODEL

The numerical code, used in this study, is ANSYS Fluent (version 14.5) [14]. The mathematical model was implemented into ANSYS Fluent code based on the finite volume method to discretize the three-dimensional compressible Naveir-Stockes equations. The hexahedral structured multi-block grids with total of 82 blocks structured mesh were designed. The blade and endwall

mesh inflations are refined near walls to get the velocity gradient in the secondary layer. A steady-state code and only one blade passage was modeled. The code was running in a parallel mode with a four-thread job density based solver.

3.1. CFD Governing Equations

The numerical simulation of compressible flows is based on the solution of the conditionally-averaged Navier- Stokes equations completed by a turbulence model equations and a model of the laminar/turbulent transition. In this solver, the 2nd-order central differencing is applied for viscous numerical fluxes. The equations of finite volume method and turbulence model and its discretization are described in ANSYS FLUENT Theory guide [14] and the basic conservative equations are described by Versteeg and Malalaskera [15].

3.2. Computational Domain and Mesh

The geometry of the blade cascade is created by ANSYS Design Modeler (14.5 version), as illustrated by Fig. 3. The computational domain for the study of the three-dimensional injection flow to linear cascade flow is consisted of one pitch endwall with a single blade periodicity channel. The blade model is 2D with the same profile in the span direction and extended from 1.0 C_{ax} upstream of the leading edge to 2.0 C_{ax} downstream of the trailing edge, in the same manner as Wan et al. [16]. The computational domain for a single pitch of the GE Energy Efficient Engine (EEE) blade is shown in Fig. 3.

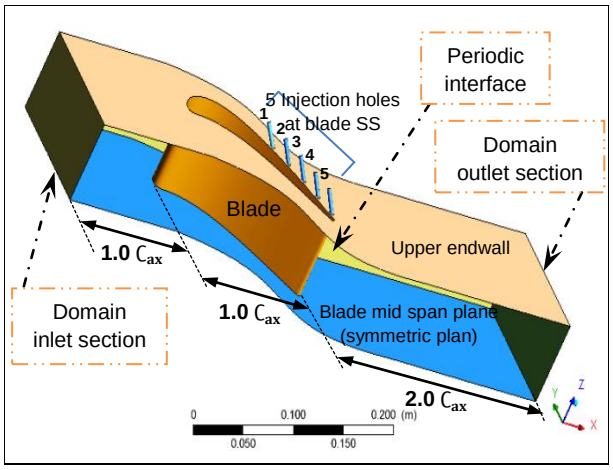

Fig. 3: The flow domain geometry

According to the law of the wall of Theodore Von Kármán [17], which states "the average velocity of a turbulent flow at a certain point is proportional to the logarithm of the distance from that point to the wall boundary of the fluid region", a non-dimensional wall distance for a wall-bounded flow, y plus (y^+), can be calculated by Fluent to precise the wall effect on the flow behavior. The density of mesh cells is increased in the vicinity of the blade wall with elements inflation and also at endwall surface with elements inflation and spanwise distribution as shown in Fig. 4 and Fig. 5 respectively.

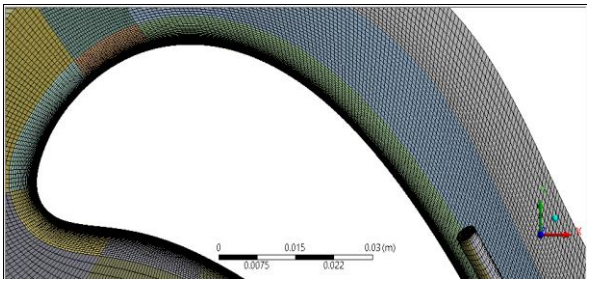

Fig. 4: The blade wall elements inflation

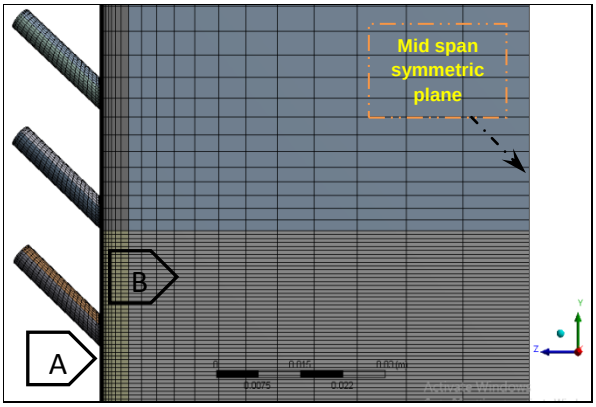

Fig. 5: Meshing, (A) Endwall inflation (B) Spanwise distribution

The initial domain grid elements were 1,816,233 elements with 641335 nodes, which include 20 edge sizings with different values. The element size is 2 x 10^{-3} m. After a series of tests and adjustments, the final adopted 3D wall-function mesh for the entire computational domain, have a total of 2.2 million of hexahedral cells.

An assumption of flow characteristics symmetry upper and lower blade mid span plane, is existing. This assumption saved the solution time cost as the computational model domain is only considered from blade mid span to blade cascade endwall.

3.3 Turbulence Models Sensitivity Study

A turbulence models sensitivity study was made to find the best accurate turbulence model which can predict a stable solution with minimum errors comparing to experimental results. Four turbulence models were tested with the same grid elements 2.2 million cells as follows;

1-The standard SST (Shear Stress Transport) k–ω,
2-The one-Equation Spalart-Allmaras,
3-The two-Equation Realizable k–ε and
4-The SST (Shear Stress Transport) Transition

The turbulence models check has been carried out to compare the result of two important flow performance factors with the experimental result as follows;

1-Total Pressure Loss Coefficient ω and
2-Total pressure coefficient C_{Pt}

3.3.1 Turbulence Models Check for Total Pressure Loss Coefficient ω

The total pressure loss coefficient, ω, of the experimental result, with the application of the same boundary conditions, is computing using Equation (3) [11]. As shown in Fig. 6, the nearest predicted result to the experimental result is counting by Spalart-Allmaras model with a tolerance of experiment result is +1.9 x 10^{-4} %. In the other side, the SST Transition Model calculates the highest tolerance of experiment result is – 0.12 %.

$$\omega = \frac{(P_{t1} - \overline{P_{t2}})}{(P_{t1} - \overline{P_2})} \quad (3)$$

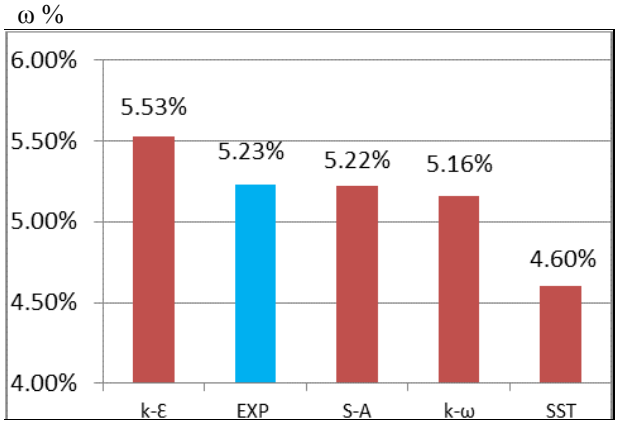

Fig. 6: Loss coefficient ω % at exit section for different turbulence models and the experiment results

3.3.2 Turbulence Models Check for Total Pressure Coefficient C_{Pt}

The total pressure coefficient, C_{Pt}, from experimental result, can be calculated from Equation (4) [11]. Fig. 7 represents, in the x axis, y – coordinate of blade cascade in pitch direction ratio to blade pitch and the total pressure coefficient distribution [11]. It is generated, by comparing the experiment result to the numerical results of the different applicable turbulence models with the same boundary conditions of the experiment study.

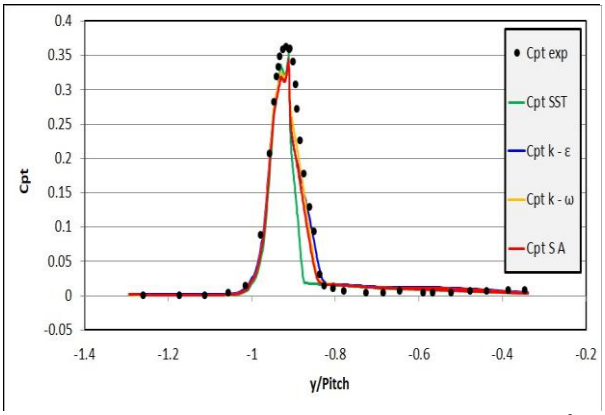

Fig. 7: Total pressure coefficient C_{Pt} with $+9.1^{\circ}$ incidence angles with different turbulence models results

$$C_{Pt} = \frac{(P_{t1} - P_t)}{(P_{t1} - \overline{P_2})} \quad (4)$$

The calculations show that, the nearest predicted result to the experiment result is that with the Spalart-Allmaras model because of a good matching between its line plot with the experiment result line plot. In the other side, the SST Transition Model calculates the highest deviated line of experiment result line plot.

According to the previous study, The Spalart-Allmaras model has been selected for CFD calculations in the progress of the current study.

3.4 Grid Dependency Study

In order to choose the suitable mesh, three mesh densities were tested with test case No. as follows:

1- 0.56 million cells, coarse grid
2- 2.2 million cells, medium grid
3- 5.1 million cells, fine grid

Simulations were carried out for the total pressure loss coefficient, ω, because of its importance to the present study. The difference in loss coefficient, ω is varied by 12.18% for the coarse grid (0.56 million cells) and 8.96% for the medium grid (2.2M), relative to the most refined grid. The mass-averaged total pressure is presented at a plane located at1.086 C_{ax} downstream blade leading edge. The loss coefficient, ω, was estimated for the three grids and depicted in Fig. 8. It shows that the loss coefficient, ω is converged with increasing the grid points. Therefore, the medium grid was selected in this study. This would be enough to capture details of the flow characteristics and based on these results, the medium grid size is considered to be sufficient for flow field predictions.

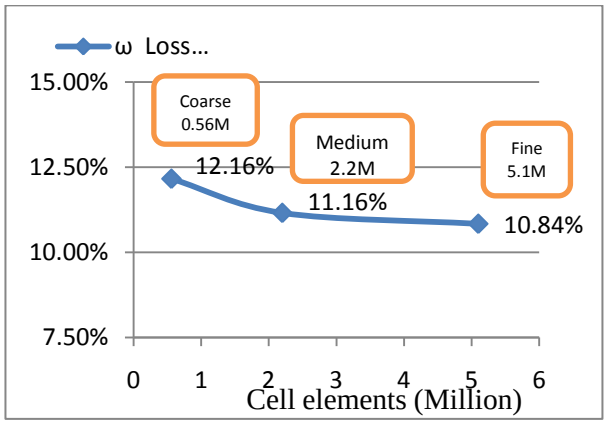

Fig. 8: Grid Dependency study for Coarse, Medium and Fine Grid

3.5. Solver Validation

Validation data are very critical to gain confidence in the calculated results. The experimental result of Ashlie et al. [11], was used for solver validation, the vertical axis is the static pressure coefficient, C_{Ps} whereas the horizontal axis is blade axial location to blade axial chord x/C_x at the blade mid span. The static pressure coefficient, C_{Ps}, is calculated by Equation (5) [11] as follows;

$$C_{Ps} = \frac{(P - \overline{P_2})}{(P_{t1} - \overline{P_2})} \quad (5)$$

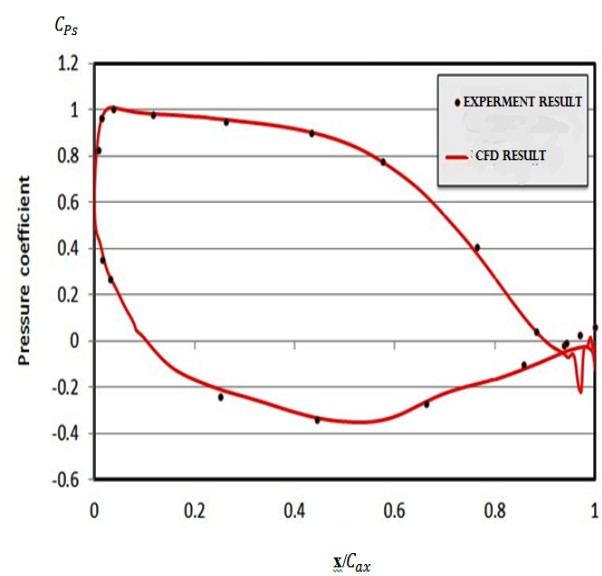

Fig. 9: Validation of CFD result with experiment result of static pressure coefficient, C_{Ps} at the blade mid span [11]

Spalart-Allmaras turbulence model results show reasonable agreement with the experimental results as shown in Fig. (9), except for some differences on the suction side and near the trailing edge, which is believed to be due to the sensitivity of the turbulence model and grid topology. Maximum y^+ of 3.3 occurs at endwall with the blade SS corner. While no valuable change in wall y^+ on blade pressure side (PS) after injection application compared to the base line. Moreover, the wall y^+ does not exceed a value of 22 on the blade cascade endwall. Spalart-Allmaras turbulence model (The current test cases turbulence model) has been extended within ANSYS FLUENT with y^+ values in the buffer layer (1< y^+<30) [14]. The calculated y^+ values emphasizes that, all 9 test cases were carried out with a stable solution by fluent calculations of flow parameters near walls of the calculation domain. For further details, see Alam El-Din et al. [21].

4. RESULTS DISCUSSION

The injection process is carried out via a set of five holes. There are two methods of injection. In the first one, all the five holes have the same inclination angle. However, in the second method, every injection hole has different inclination angle. A wide range of injection hole inclination angles, from 15° to 90° (from almost the direction of main flow to perpendicular direction to the main flow direction), was studied and compared with the baseline case (without injection). The selected inclination angles β_h injection holes are as shown in Table 2. Eight test cases are presented to investigate the effect of changing the injection hole inclination angle on flow performance with injection location at blade SS as shown in Fig. 3 and blowing ratio, $M_{h-inlet}$ = 0.6. Meanwhile, the injection holes orientation angles (α_h) for each test case location were selected to obtain flow direction matching between the injection flow and main passage flow and this to avoid disturbance or increasing losses of main flow. The values of holes orientation angles are shown in Table 3 for all test cases.

Table 2: Tested inclination angles β_h

Case No.	inclination angles β_h	
1	All five injection holes have the same inclination angle - method (1)	15°
2		30°
3		45°
4		60°
5		75°
6		90°
7	Different inclination angle for each injection hole - (method (2)	41° (averaged)
8		67.5° (averaged)

Table (3) Injection hole configuration and inlet conditions

Inclination angle		15	30	45	60	75	90	Mix. Ave. 41°	Mix. Ave. 67.5°
X (mm)	x_1	93	93	93	93	93	93	93	55
	x_2	104	104	104	104	104	104	104	76
	x_3	114	114	114	114	114	114	114	93
	x_4	122.9	122.9	122.9	122.9	122.9	122.9	122.9	108
	x_5	131.2	131.2	131.2	131.2	131.2	131.2	131.2	126
Y (mm)	y_1	0	0	0	0	0	0	0	45
	y_2	-20	-20	-20	-20	-20	-20	-20	24.8
	y_3	-40	-40	-40	-40	-40	-40	-40	1
	y_4	-60	-60	-60	-60	-60	-60	-60	-20
	y_5	-80	-80	-80	-80	-80	-80	-80	-50
Z (mm)	z_1	76.2	76.2	76.2	76.2	76.2	76.2	76.2	76.2
	z_2	76.2	76.2	76.2	76.2	76.2	76.2	76.2	76.2
	z_3	76.2	76.2	76.2	76.2	76.2	76.2	76.2	76.2
	z_4	76.2	76.2	76.2	76.2	76.2	76.2	76.2	76.2
	z_5	76.2	76.2	76.2	76.2	76.2	76.2	76.2	76.2
β_h°	β_{h1}	15	30	45	60	75	90	60	75
	β_{h2}	15	30	45	60	75	90	50	75
	β_{h3}	15	30	45	60	75	90	40	67.5
	β_{h4}	15	30	45	60	75	90	30	60
	β_{h5}	15	30	45	60	75	90	25	60
α_h°	α_{h1}	-58	-58	-58	-58	-58	-58	-58	-28.5
	α_{h2}	-62.5	-62.5	-62.5	-62.5	-62.5	-62.5	-62.5	-52
	α_{h3}	-63.8	-63.8	-63.8	-63.8	-63.8	-63.8	-63.8	-56.7
	α_{h4}	-66.5	-66.5	-66.5	-66.5	-66.5	-66.5	-66.5	-60
	α_{h5}	-67	-67	-67	-67	-67	-67	-67	-63
D_h (mm)	D_{h1}	4	4	4	4	4	4	4	3.5
	D_{h2}	4	4	4	4	4	4	4	3.5
	D_{h3}	4	4	4	4	4	4	4	3.5
	D_{h4}	4	4	4	4	4	4	4	3.5
	D_{h5}	4	4	4	4	4	4	4	3.5
$M_{h-inlet}$		0.6	0.6	0.6	0.6	0.6	0.6	0.552	0.312
MFR_h (g/s)	MFR	1	1	1	1	1	1	1.5	0.75
	MFR	1	1	1	1	1	1	1.2	0.5
	MFR	1	1	1	1	1	1	0.9	0.5
	MFR	1	1	1	1	1	1	0.65	0.5
	MFR	1	1	1	1	1	1	0.35	0.35

4.1 Injection and Main Flow Streamlines Interaction

The interaction between injection and mian flow streamlines is shown in Fig. 10. Flow streamlines are colored by flow inlet source in the flow domain for the baseline and eight test cases with different injection holes inclination angles.

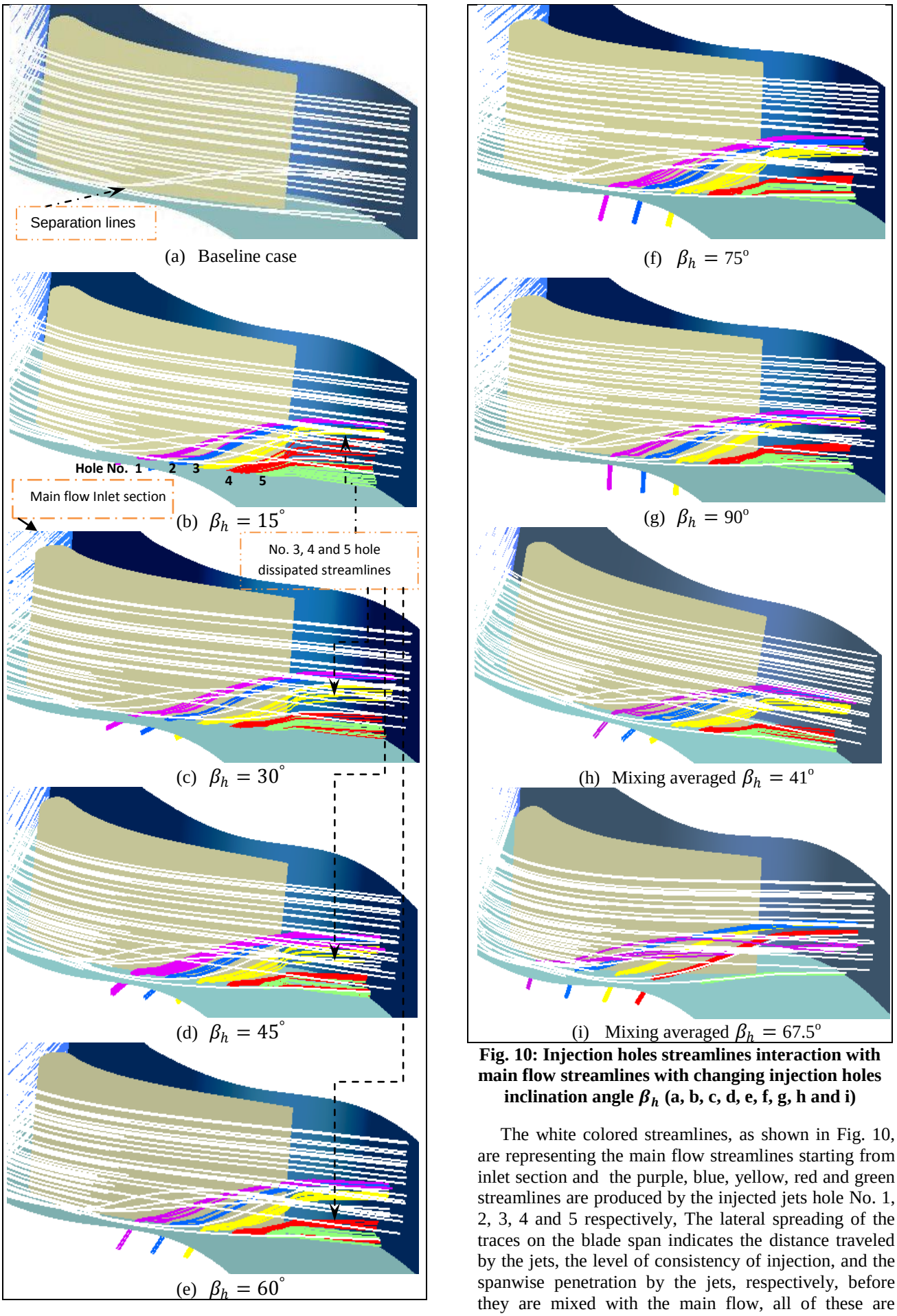

Fig. 10: Injection holes streamlines interaction with main flow streamlines with changing injection holes inclination angle β_h (a, b, c, d, e, f, g, h and i)

The white colored streamlines, as shown in Fig. 10, are representing the main flow streamlines starting from inlet section and the purple, blue, yellow, red and green streamlines are produced by the injected jets hole No. 1, 2, 3, 4 and 5 respectively, The lateral spreading of the traces on the blade span indicates the distance traveled by the jets, the level of consistency of injection, and the spanwise penetration by the jets, respectively, before they are mixed with the main flow, all of these are

dependent factors on injection holes inclination angle β_h.

The main flow streamlines separation is clearly appeared at the blade SS (suction side) as shown in Fig. 10 (a). The injection flow streamlines of hole No. 3 (yellow colored streamlines) with high inclination angles, ($\beta_h = 60^{\circ}$, $\beta_h = 75^{\circ}$, $\beta_h = 90^{\circ}$and mixing averaged $\beta_h = 67.5^{o}$), can significantly penetrate the main flow deeply to almost quarter blade span without notable dissipation as indicated) in Fig. 10 (e) to (g) and Fig 10 (i) compared to the same streamlines (yellow colored) in Fig. 10 (b) to (d) and Fig. 10 (h). Thus, these injection flow streamlines with low injection holes inclination angles, ($\beta_h = 15^{\circ}$, $\beta_h = 30^{\circ}$, $\beta_h = 45^{\circ}$ and mixing averaged $\beta_h = 41^{o}$), are easily swept with the main flow as soon as they are ejected.

The two aft holes streamlines, (h_4 and h_5), are widely separated with deflection downstream the blade TE with injection holes inclination angles $\beta_h = 15^{\circ}$, as shown in Fig. 10 (b), which indicates an existence of strong guided streamlines with small cute inclination angel (almost parallel with the main flow streamlines direction) which can been separated widely and affected on more volume of flow with injection location near the exit section and hence increase exit total pressure losses.

4.2 Static Pressure and Blade Loading

As shown in Fig. 11 (a), Due to the adverse pressure gradient on the suction surface downstream of the minimum C_p, there is the potential of boundary layer separation from the suction-side blade surface near the trailing edge and this represents a major source of profile losses in the blade passage.

By injection application, the pressure distribution does not change along most of the blade PS span or height except near blade T.E. with endwall corner, the static pressure on the blade SS increases slightly at the trailing edge due to the expansion at the trailing edge region. The injection flow effect is clearly notable in Fig. 11 (b) to (i), by increasing local static pressure contours at the aft blade SS as a result of the jet momentum spanwisely sweeping the pressure contours away from endwall.

By injection with mixing high averaged inclination angles of injection holes, $\beta_h = 67.5^{o}$, the low static pressure zone (blue colored) on blade SS is shrinking away from endwall and concentrated around blade mid span region as shown in Fig. 11 (b) to (g). Also, the area of relatively high pressure blade T. E. is increased by the effect of with changing injection holes inclination angle $\beta_h = 15^{\circ}$ Fig. 11 (b), comparing to other cases with injection as shown in Fig. 11 (i).

The jet penetration effect is clearly seen in blade aft suction side with endwall corner by injection application with injection holes inclination angle $\beta_h = 60^{\circ}$, $\beta_h = 75^{\circ}$ and $\beta_h = 90^{\circ}$ as shown in Fig. 11 (e) to (g).

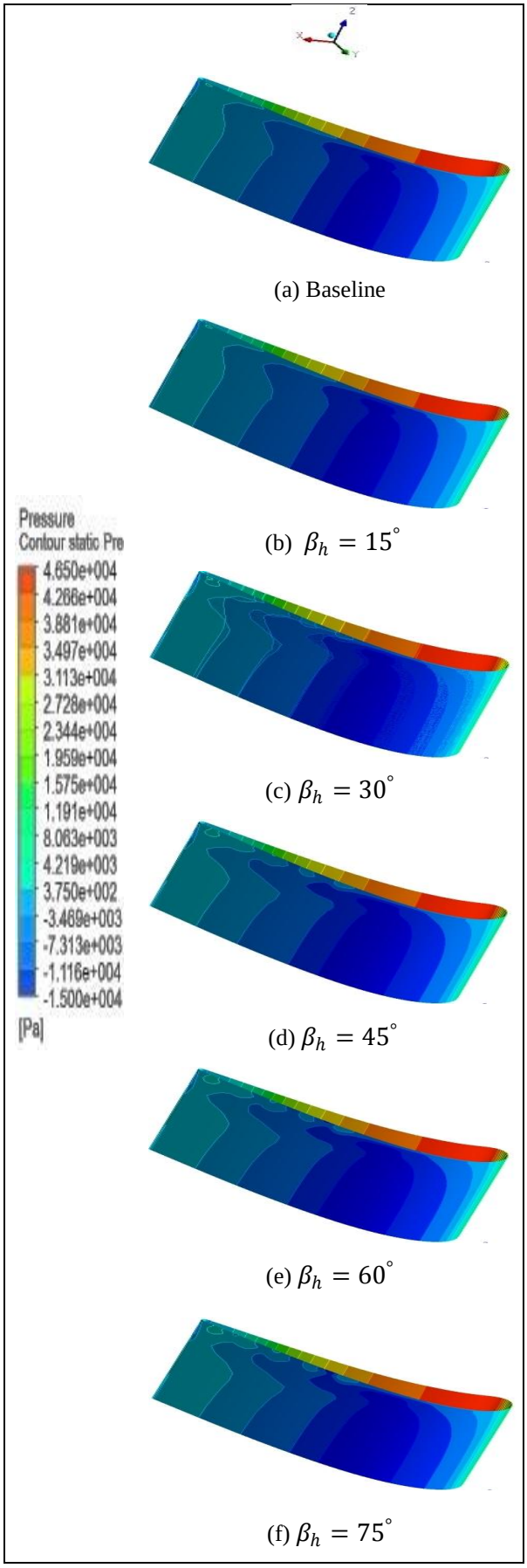

(a) Baseline

(b) $\beta_h = 15^{\circ}$

(c) $\beta_h = 30^{\circ}$

(d) $\beta_h = 45^{\circ}$

(e) $\beta_h = 60^{\circ}$

(f) $\beta_h = 75^{\circ}$

Fig. 11: Local static pressure on blade SS with changing injection holes inclination angle β_h (a, b, c, d, e and f)

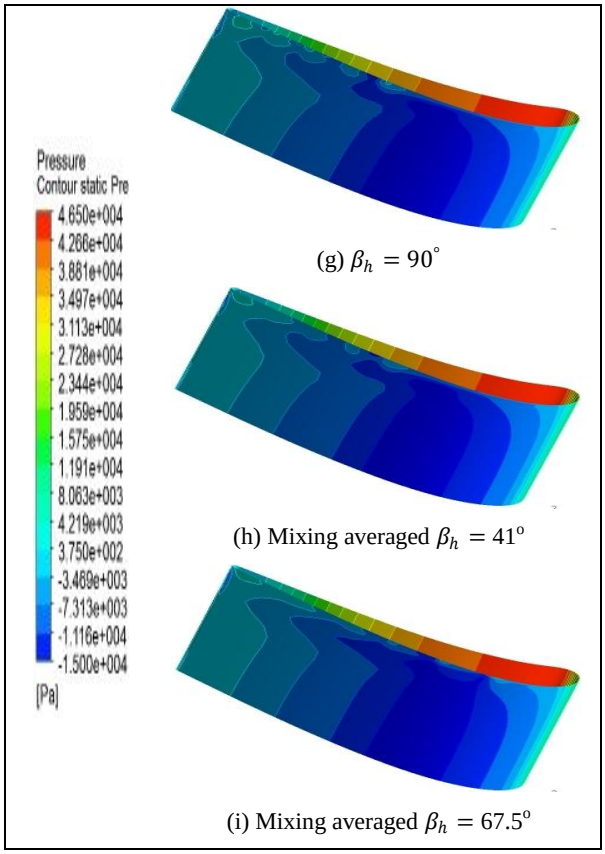

Fig. 11: (cont.) Local static pressure on blade SS with changing injection holes inclination angle β_h(g, h and i)

Results of blade loading ratio for base line and different injection holes inclination angle β_h, calculated by CFD, are shown in Fig. 12. It indicates that, in all chosen injection holes inclination angle β_h, there are an apparent increasing in blade loading comparing to baseline test case.

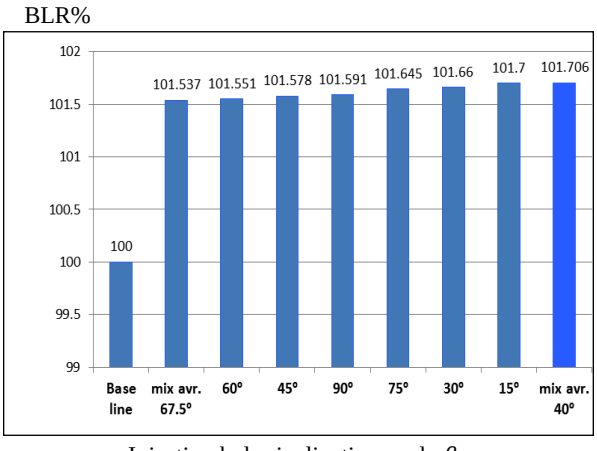

Fig. 12: Blade loading ratio (BLR %) with changing injection holes inclination angle β_h

By injection application with low mixing inclination angle of injection holes, averaged $\beta_h = 41^o$, an increment of 1.7١ % in blade loading is obtained. And generally, Fig. 12 indicates that, the blade loading is increasing with the decreasing of inclination angle. The test case of low mixing inclination angle is produced to gain a higher blade loading meanwhile keeping the injection flow reduces the flow losses.

4.3 Exit Total Pressure and Losses

Figure 13 represents the total pressure contours downstream blade T. E. (108.6% axial chord) with changing the injection holes inclination angle β_h comparing to baseline test case. The peaks and valleys in the endwall locally decrease or increase the total pressure respectively. The high pressure loss in flow field is colored with deep blue. The total pressure fields at the exit of the blade, the secondary flows and the vortex can be clearly identified as low total pressure region.

Three main phenomenons can express the level of pressure losses in Fig. 13. First, the overall red to blue colors of the exit area which indicates the total pressure drop through the flow passage. Second, the bigger area of pressure contours core of the suction side leg vortex and the passage vortex, near the suction surface, indicates more pressure losses are created. The third phenomenon is the ratio of spanwise distance to blade span ratio S_z of this core center to the endwall. Losses increase as this center moves nearer to the mid-span [18].

A high loss flow region appears on the suction side at the blade trailing edge, which is contributed by the secondary flow. Fig. 13 (a) shows the total pressure loss distribution contour at the blade outlet without flow injection with spanwise distance of the pressure contour core center to the endwall to the blade span S_z = 17.5%, and Fig. 13 (b) to (i) shows the total pressure loss distribution contour at the blade outlet with flow injection with changing injection holes inclination angle β_h.

The flow losses are increased as the separation lines for the suction side leg vortex and the passage vortex on the suction surface move nearer to the mid-span. It could be seen that, the flow loss is reduced with flow injection from blade with injection holes inclination angle $\beta_h = 30^\circ$, as shown in Fig. 13 (c) with S_z = 18%. Also, Fig. 13 (c) to (g) shows that the main flow exit total pressure is generally increased meanwhile, the loss core is deeply been condensed with blue which indicates an increasing loss region at blade SS with increasing the holes inclination angle to $\beta_h = 90^\circ$.

Comparisons of the baseline case results Fig. 13 (a) to the injection cases at blade SS with changing injection holes inclination angle β_h Fig. 13 (b) to (i), flow exit section changes the secondary flow to keep the passage vortex close to the endwall and by reducing the depth of the associated loss core as shown in Fig. 13 (b) and (d). Injection at passage flow exit section only seems to thicken the exit boundary layer and give a strong indication that injection upstream of the separation lines can significantly change the secondary flow. To insure this point, the effect of holes located at passage flow exit section, Fig. 13 (d) shows, the results clearly keep S_z = 21.5%.

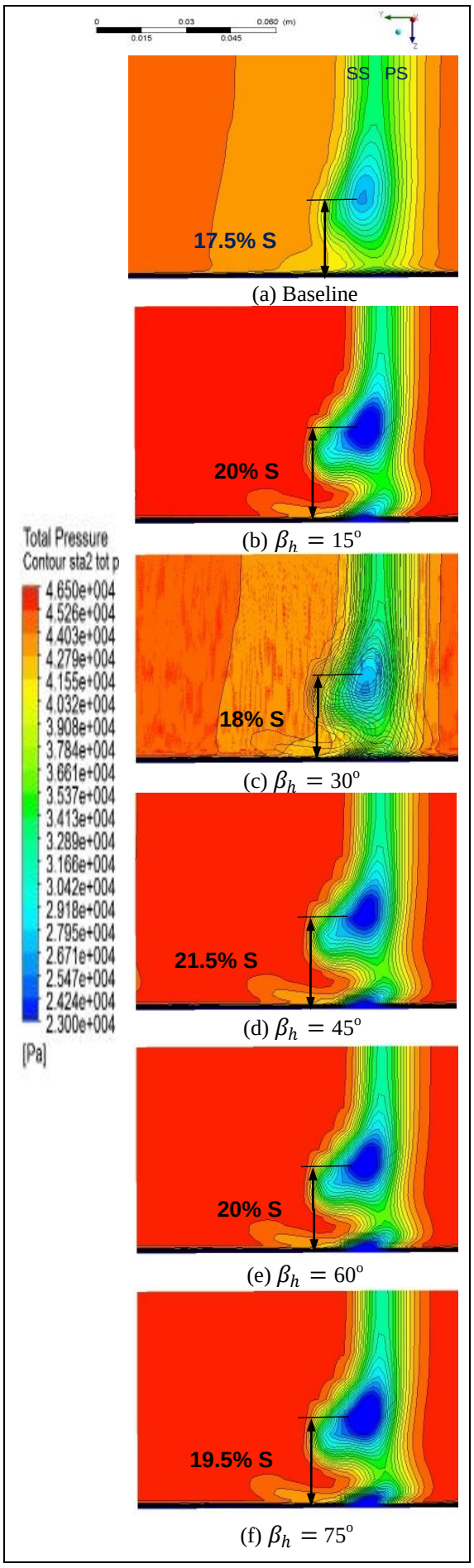

Fig. 13: Total pressure contours downstream blade T. E. (108.6% axial chord with changing injection (holes inclination angle β_h (a, b, c, d, e, f, g, h and i)

The results introduce that, this injection location at blade SS, reduces the total pressure loss across the blade passage by weakening the endwall cross flows and passage vortex, and hence the location chosen for injection is very important in this respect. Fig. 13 shows the great difference of pressure field and provides evidence by how strongly the secondary flows deflect some jets flow because of their injection holes inclination angle β_h.

By checking the results carefully, it is clear that the injection holes inclination angle $\beta_h = 30^\circ$ is more effective to suppress the secondary flow loss near the end-wall with S_z = 18% as shown in Fig. 13 (c).

The produced test case, with high mixing averaged inclination angle of $\beta_h = 67.5^o$, is giving the best result in loss reduction by minimizing low pressure contours core area and relatively decrease spanwise core distance to endwall with S_z = 20.5% as shown in Fig. 13 (i) and hence, an increasing in exit total pressure is gained.

The peak flow loss of secondary flow could be increased by 0.56 % with injection application with injection holes inclination angle $\beta_h = 15^\circ$, as shown in Fig. 14. The result indicates that the secondary loss growth is slightly influenced by the jet-flow with injection holes inclination angle $\beta_h = 15^\circ$ that injection flow is strongly affecting and penetrates the passage

flow exit section with this small inclination angle. As it could be seen, the secondary loss reduction is almost same when the jets flow with injection holes inclination.

It can be noted that as shown in Fig. 14, the injection flow with injection holes inclination angle $\beta_h = 30^\circ$ and with mixing injection holes high averaged inclination angle $\beta_h = 67.5^o$ will be more effective methods to suppress secondary flow development in a maximum loss reduction obtained, about ٢.١ % comparing to the baseline test case angle $\beta_h = 75^\circ$ and with injection holes inclination angle $\beta_h = 90^\circ$.

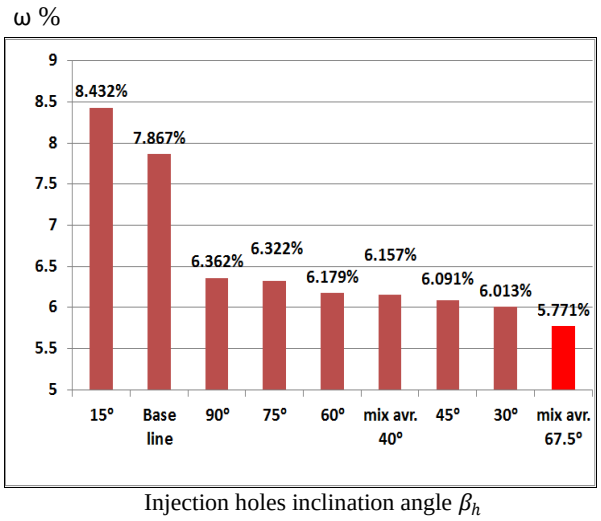

Fig. 14: Total pressure loss coefficient ω % with changing injection holes inclination angle β_h

5. ECONOMIC REVIEW

The economic factor of aviation fuel is of a great concern, which worries commercial airlines. The current daily worldwide jet fuel consumption is about 5.6 million barrels per day, or 5.8 percent of total global oil consumption and the demand for fuel could increase by as much as 2.7 million more barrels per day by 2030, OPEC [19]. This may make the achieved result of 2% in the current study, either loss reduction or gain in blade loading, leads to a jet fuel consumption reduction of 41 million barrel per year or a jet fuel cost reduction of 3.2 billion US$ per year (with averaged 2018 jet fuel barrel price of 87.3 US$), IATA [20], which can consider a valuable achievement in the aviation industry. This is only in the field of aviation, not to mention the fuel saving in other land uses of the gas turbine engine. Also, it serves with the world need for decreasing carbon emissions to keep clean atmosphere.

6. CONCLUSIONS

The important conclusions can be drawn from this thesis are:

1- Endwall jets located towards the suction side of a turbine blade passage were effective in altering the path of the pressure-side leg of the corresponding blade horse shoe vortex and leads to improve the mixing of control flow and main flow separation and hence produce increasing in static local pressure on pressure side (1.71% increasing in blade loading) comparing to the base line case and hence save more power for turbine rotation.

2- The total exit pressure readings have a significant decreasing in their values with injection inclination angle $\beta_{h4} = 15^\circ$, which deteriorate the flow losses with 0.57% loss growth and record the worst reading for flow losses comparing to the baseline result. It indicates that injection inclination angle close to main flow direction cause a harmful effect to flow performance, in such way, the total flow velocity is increasing at flow exit section and hence it leads to total exit pressure drop then flow passage is loss increasing.

3- The blade loading does not increase in linear relation with increasing injection inclination angle and an existence of inflation inclination angle is exist, with value around $\beta_h = 60^\circ$, the flow reverse its influence with blade loading, as shown in Fig. 12.

4- The flow loss does not react in linear relation with increasing or decreasing injection inclination angle and an existence of inflation inclination angle is exist, with value around $\beta_h = 30^\circ$, where the flow reverse its influence with flow losses, as shown in Fig. 14.

5- the new injection arrangement technique has proved its effectiveness in suppressing flow losses by loss reduction result 2.1% less than baseline test case and that is implemented by individual change for each hole injection hole inclination angle, as in test case with mixing averaged $\beta_h = 67.5^o$ with injection location at blade SS. This case can be applied on turbojet engine design while the fluid energy is a higher priority aspect in engine design.

6- The blade loading and flow losses are changing independently with injection parameters change, i.e. the increasing in the blade loading, for certain injection arrangement, does not reflect a reduction in flow losses. The test case with mixing averaged $\beta_h = 67.5^o$ and test case with mixing averaged $\beta_h = 41^o$ are considered the best simultaneously results for both two important flow factors and both cases can be applied on turbofan engine design design while mechanical and fluid energies are simultaneously required.

7- The new injection arrangement technique has proved its effectiveness in increasing blade loading 1.85 % comparing to baseline test case, and that is implemented by individual change for each hole injection location, hole inclination angle, and hole mass flow rate as in test case with mixing averaged $\beta_h = 41^o$ with injection location at blade aft half SS. This case can be applied on turboshaft or turboprop engine design, while the mechanical energy is a higher priority aspect in engine design.

8- All selected test cases gave positive different readings with respect to blade loading comparing to baseline test case, which proves the great effectiveness of injection location at blade SS on increasing blade loading.

9- The injection flow, in most of test cases, was deflected and dissipated because of high inlet pressure boundary conditions of basically selected experimental test case to validate and study.

NOMENCLATURE

A Area [m^2]
C Blade chord [m]
C_{ax} Blade axial chord [m]
C_L Lift coefficient $C_L = 2L/\rho A v^2$
C_{Ps} Static pressure coefficient $C_{Ps} = (P - \overline{P_2}) / (P_{t1} - \overline{P_2})$
C_{Pt} Total pressure coefficient $C_{Pt} = (P_{t1} - P_t) / (P_{t1} - \overline{P_2})$
D_h Injection hole diameter [m]
i Incidence angle [deg], $i = \beta_1 - \beta_{1,des}$
k Turbulent kinetic energy per unit of mass [Joule/kg], $k = \frac{1}{2}(u^2 + v^2 + w^2)$
ṁ Mass flow, kg/s
M Mach number
$M_{h-inlet}$ Blowing ratio, $M_{h-inlet} = (\dot{m}_{inj} / A_{holes}) / \rho_\infty . U_\infty$
PR Pressure Ratio, PR = $P_{t1}/\overline{P_2}$
P Pressure [Pa]
$\bar{P}$ Area-averaged static-pressure [Pa]
$\overline{P_t}$ Area-averaged total-pressure [Pa]
Re Reynolds number, Re = $\rho U_1 C_{ax}/\mu$
S_z The ratio percentage of spanwise distance to the blade endwall relative to blade span, $S_z = \frac{z}{S} * 100\%$
u Velocity at x – coordinate [m s^{-1}]
U Total velocity [m s^{-1}]
v Velocity at y – coordinate [m s^{-1}]
V Volume flow rate, m^3/sec
w Velocity at z – coordinate [m s^{-1}]
x Chordwise (axial) coordinate
y Pitchwise coordinate
z Spanwise coordinate
y^+ Dimensionless wall distance (y plus), $y^+ = \frac{u_T . y}{\nu}$

Subscripts

1 Cascade inlet value
2 Cascade exit value
ax Axial
des Design value
h Injection hole
holes All injection holes
i Isentropic value
in Inlet
inj Injection flow
out Outlet
s Static conditions
t Total conditions
∞ Mainstream air at inlet conditions
1, 2.., 5 Injection hole number

Greek symbols

α_h Injection hole orientation angle
β Relative flow angle [deg]
β_h Injection hole inclination angle
δ Boundary layer thickness [in]
ε Rate of dissipation of turbulent kinetic energy per unit mass [Joule/kg]
λ Second viscosity (relates stresses to the volumetric deformation) [Pa.s]
ρ Density [kg/m^3]
ω Loss coefficient, $\omega = (P_{t1} - \overline{P_{t2}}) / (P_{t1} - \overline{P_2})$

Abbreviations

2D Two Dimensions
3D Three Dimensions
AR Area Ratio, injection hole area outlet to area inlet (A_{out}/A_{in})
BLR% Blade Loading Ratio ($\frac{L.}{L_{baseline}} . 100\%$)
CFD Computational Fluid Dynamics
EEE Energy Efficient Engine
EXP Experiment
GE-E^3 General Electric - Energy Efficient Engine
HPT High Pressure Turbine
IATA International Air Transport Association
LCTR Large Civil Tilt Rotor
L.E. Leading Edge
MFR Mass Flow Rate
OPEC Organization of the Petroleum Exporting Countries
SA Spalart-Allmaras
SS Suction Surface
STA2 Station at Passage flow Exit section (x = 108.6% C_{ax})
T.E. Trailing Edge
US$ United states Dollar

REFERENCES

1- Nicole V. A, Ralph J V, Karen A. F. and Ryan M. S. "Secondary Flow Measurements in a Turbine Passage with Endwall Flow Modification" ASME Turbo EXPO (2000).
2- Gregory-Smith D. G. and Okan B. M. 'The Estimation of Secondary Flows and Losses in Turbines", Proceedings of 1st European Turbomachinery Conference - Fluid Dynamic and Thermodynamic Aspects, Germany. (1995).
3- Langston L.S. "Crossflows in a turbine cascade passage" ASME Journal Engineering. Power, 102 (4), pp. 866-874. (1980).
4- Denton J.D. and Cumpsty N.A. "Loss mechanisms in turbomachines"; Institue of Mechanical Engineers; Paper No.: C260/87, (1987).
5- Sharma, O. P., Joslyn, H. D. & Dring, R. P. "Redistribution of an inlet temperature distortion in an axial flow turbine stage", AIAA J. Propulsion and Power Vol. 5(No. 1): 64-71. (1989).
6- Dixon S.L., Hall C.A. "Fluid Mechanics and Thermodynamics of Turbomachinery" 6th Edition. Burlington: Elsevier Inc., (2010).
7- Satta F. and Tanda G. "Effect of discrete-hole arrangement on film-cooling effectiveness for the endwall of a turbine blade cascade" Applied Thermal Engineering 91, 507e514. Genova, Italy, (2015).
8- Leylek J. H. and Zerkle R. D. "Discrete-Jet Film Cooling: A Comparison of Computational Results with Experiments," ASME Journal of Turboma-chinery, Vol. 116, pp. 358-368, (1994).

9- Jian Pu A, Jian-hua Wanga, “An experimental investigation of geometric effect of upstream converging slot-hole on end-wall film cooling and secondary vortex characteristics” Experimental Thermal and Fluid Science 69 (2015) 58–72, China, (2015).
10- Qing Pan, Huimin Tang and Jiangtao Bai, “Numerical analysis of film cooling characters on a turbine non-axisymmetric contoured endwall” AIAA Thermophysics Conference 2015-2814, Dallas, TX., (2015).
11- Ashlie B. McVetta, Paul W. Giel and Gerard E. Welch “Aerodynamic Investigation of Incidence Angle Effects in a Large Scale Transonic Turbine Cascade”NASA/TM—2013-218070/REV1, (2014).
12- Timko L. P., “Energy Efficient Engine High Pressure Turbine Component Test Performance Report,” NASA/CR—1984-168289, (1984).
13- Alam El-Din A. M. , El-Sawaf I. A. , El-Abady A. A. , Hassan Y. K. "An Investigation of the Controlling Methods for the Secondary Losses in Turbine Blades" The Research Journal of Shebin El-kom Faculty of Engineering, Minoufiya University, Vol. 34 No.2 (April 2011).
14- “ANSYS FLUENT Theory Guide" ANSYS, Inc., www.ansys.com, Release 14.5, (2013).
15- Versteeg H.K., Malalasekera W. “An Introduction to Computational Fluid Dynamics The Finite Volume Method” Pearson Education Limited, Glasgow,2nd edition, (2007).
16- Wan Aizon W Ghopa, Zambri Harun, Ken-ichi F. and Takemitsu M. “Aero-Thermal Performances of Leakage Flows Injection from the Endwall Slot in Linear Cascade of High-Pressure Turbine” Journal of Thermal Science Vol.24, No.1, (2015).
17- Von Kármán, Theodore “Mechanical Similitude and Turbulence” Tech. Mem. NACA, no. 611, (1931).
18- Acharya S. and Mahmood G. “Gas Turbine Hand Book- sec. 4.3 Turbine blade aerodynamics” A Handbook of Land, Sea and Air Applications by Claire Soares, publisher Butterworth Heinemann, BH, McGraw Hill, (2006).
19- OPEC, Monthly Oil Market Report, 13 November (2018).
20- IATA, Jet fuel price monitor publication, www.iata.org/publications/economics/fuel-monitor/Pages/index.aspx, (December 2018).
21- Alam El-Din A. M., El-Ghandour M. E., Hassan Y. K. “A Numerical Study on the Effect of Air Injection on Secondary Flow in a Turbine Cascade” A Doctorate Thesis, Faculty of Engineering, Port Said University, Egypt (2018).

دراسة رقمية لتأثير تغيير زوايا ميل حقن جدارى على أداء مصفوفة ريش توربينة عالية الضغط

ملخص البحث

يتناول هذا البحث دراسة رقمية لمحاكاة التحكم فى المفاقيد الثانوية لريش التوربينات الناشئة بشكل رئيسى عن إصطدام تيار الإنسياب الرئيسى الداخل للمائع بالحافة الامامية للريشة و الذى بدوره ينتج عنه تيارات دوامية مع جانب الضغط والسحب للريشة ، بما يعرف بدوامة حدوة الحصان التى تولد إختلاف ضغط المائع على إمتداد الخطوة وتسبب فى إمكانية حدوث إنفصال للطبقة الجدارية للهواء عن سطح الريشة و من ثم تقليل الكفاءة الكلية للتوربينة. تم فى هذه الدراسة التحكم فى المفاقيد الثانوية من خلال حقن هواء بزوايا ميل مختلفة لمنفثات الحقن و مباشرة على ثقوب جدارية تحيط بمسار الهواء بين ريشتين متتاليتين ومن ثم دراسة تأثير هذا الحقن على الضغوط الكلية فى مقطع الخروج له ذا المسار و الضغوط الاستاتيكية على سطحى الريشة . و لمقارنة النتائج تم إختيار بحث يشمل نتائج عملية كافية لريش توربينية و ذلك لإختبار تطابق نتائج برنامج حسابات ديناميكا الموائع ، تم إستخدام برنامج ANSYS Fluent (version 14.5) و ذلك لتصميم مجال الإنسياب لريشة مختارة و بعد التأكد من تطابق النتائج تم إختبار تفاعل الإنسياب الرئيسى لتدفق الهواء حول ريشة التوربينة و تم تطبيق ترتيبات حقن هواء جديدة ، تشمل تغيير الزوايا المركبة لكل منفث حقن على حدة و المكونة من زاوية ميل و زاوية توجيه لمنفث الحقن ، و قد تبين بعد عمل إختبارات تشمل تغيير ترتيبات حقن المنفثات أن هناك نتائج مرضية لبعض ترتيبات الحقن تصل إلى زيادة تحميل الريشة إلى ١.٧١ % و تخفيض المفاقيد الثانوية بنسبة ٢.١% مقارنة بحالة الإختبار بدون حقن و هذه النتائج الإيجابية تحدث مع وجود نقط حقن الهواء بجانب السحب للريشة فى المسار المختبر و تبين أن هذه النقط لحقن الهواء تعمل بنجاح على تباعد مسار الدوامات الهوائية و تقلل من تأثير انفصال الطبقة الجدارية على جانب السحب للريشة ، وأيضاً مع هذا التعديل يظهر تأثير ملحوظ على زيادة الضغوط الاستاتيكية على جانب الضغط للريشة الذى يؤثر بدوره مباشرة على زيادة الدفع (التحميل على ريش التوربينة) اللازم للحركة الدورانية لقرص التوربينة و بعد عمل دراسة إقتصادية لإستهلاك الوقود النفاث عالميا ، تبين أن توفير زيادة ٢% فى تحميل ريشة التوربينة أو فى تقليل المفاقيد الثانوية قد يؤدى إلى توفير ٣.٢ مليار دولار أمريكى سنويا من إستهلاك الوقود النفاث عالمياً ، و ذلك بالإضافة إلى التوفير فى إستهلاك وقود المحركات التوربينية الأرضية وأيضاً تقليل الإنبعاثات الكربونية على الغلاف الجوى و من ثم الحفاظ على بيئة الأرض.

،